ORGANOMETALLICS

Article

Cite This: *Organometallics* XXXX, XXX, XXX−XXX

pubs.acs.org/Organometallics

C−H Nickelation of Aryl Phosphinites: Mechanistic Aspects

Loïc P. Mangin and Davit Zargarian*

Département de chimie, Université de Montréal, Montréal, Québec, Canada H3C 3J7

Supporting Information

ABSTRACT: The present report describes the results of a combined experimental and computational study on the mechanism of aryl phosphinite cyclonickelation. The reaction of ArOP(*i*-Pr)$_2$ with $[(i\text{-PrCN})NiBr_2]_n$ proceeds more readily in acetonitrile relative to toluene; this is because the greater nucleophilicity of acetonitrile toward Ni stabilizes a more reactive acetonitrile adduct bearing one phosphinite ligand (as opposed to two). A sufficiently strong external base such as Et_3N serves to quench the HBr generated at the nickelation step, thus allowing isolation of the cyclonickelated species. However, nickelation tests conducted in the absence of external base revealed that D/H scrambling occurs at the ortho positions of $C_6D_5OP(i\text{-Pr})_2$, implying that the cyclonickelation proceeds independently of the base. Thus, the main role of the external base is to prevent protonation of the Ni−aryl moiety formed via C−H nickelation. Tests have also shown that nickelation rates are affected by the quantity of the base used: the presence of more than 1 equiv of Et_3N generates the less reactive biphosphinite complex *trans*-$\{PhOP(i\text{-Pr})_2\}_2NiBr_2$, thus inhibiting the desired C−H nickelation. Experimental studies have shown that nickelation is faster with aryl phosphinites bearing electron-donating substituents (Hammett slope $\rho \approx -4$) and the proton transfer is rate limiting (KIE ≈ 11). The activation parameters were found to be $\Delta H^{\ddagger}$ = 17.7 kcal mol^{-1} and $\Delta S^{\ddagger}$ = −27.1 cal mol^{-1} K^{-1}. DFT analyses have provided support for these findings and suggest that aryl phosphinite C−H nickelation proceeds via an ion-pair-assisted deprotonation.

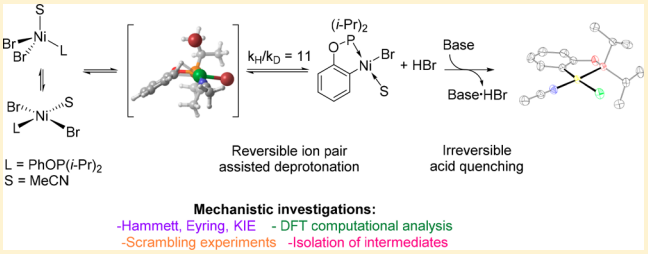

INTRODUCTION

The past decade has witnessed an increasing number of reports that disclose Ni(II)-catalyzed protocols for the direct functionalization of unactivated C−H moieties. Such non-redox-type C−H metalation processes, followed by functionalization, are facilitated by the use of at least one directing group (DG) that serves the purpose of binding to the Ni(II) center and facilitating its encounter with the C−H moiety. This type of metalation by chelation also helps determine the regiochemistry of the functionalization, which is likely controlled by the relative stabilities of the nickelacycles generated in the C−H nickelation step. In this context, the most commonly used DGs are mono- and bidentate auxiliaries based on imine-type donors, such as 2-pyrimidyl anilines (monodentate)[1] and benzamido quinolones and pyridines (bidentate),[2] which were popularized by the groups of Ackermann and Chatani, respectively. Another effective DG is pyridine oxide.[3]

In contrast to the significant progress registered in Ni(II)-catalyzed direct functionalization of unactivated C−H bonds, there is relatively little concrete mechanistic knowledge of how these processes work.[4] The main reason for this paucity of mechanistic knowledge is that most efforts to date have focused on developing one-pot protocols that combine the chelation, metalation, and functionalization steps. While such a one-pot approach is attractive from a practical point of view, it bypasses the detection and isolation of reaction intermediates and foregoes the chance to improve our understanding of reaction mechanisms. Ideally, therefore, systematic efforts are needed to isolate model cyclonickelated complexes and delineate the factors that favor various steps of the C−H functionalization process.

The above considerations and our group's longstanding interest in organonickel chemistry[5] inspired us to investigate the preparation of thermally stable cyclonickelated species via C−H nickelation and study the direct functionalization of the resulting Ni−hydrocarbyl moiety. A search of the literature revealed that most cyclonickelated complexes accessible via C−H nickelation are stabilized by pincer-type ligands.[6] Our experience with the facile C−H nickelation of POCOP-type pincer ligands featuring aryl and alkyl phosphinite donor moieties[7] encouraged us to test the reactivities of substrates bearing a single phosphinite DG. Initial tests showed that alkyl phosphinites were insufficiently reactive, whereas aryl phosphinites underwent relatively facile C−H nickelation. Thus, we succeeded in accessing the isolable and thermally stable ortho-metalated complexes $\{(\kappa^P,\kappa^C\text{-ArOPR}_2)Ni(\mu\text{-Br})\}_2$ and $(\kappa^P,\kappa^C\text{-ArOPR}_2)Ni(L)Br$ (Chart 1; R = *i*-Pr) and then studied their structures, stabilities, and reactivities with electrophiles.[8]

In addition to the aforementioned promising reactivities of aryl phosphinites, we should also note that these substrates present many advantages in the context of the proposed

Received: December 12, 2018

DOI: 10.1021/acs.organomet.8b00899
Organometallics XXXX, XXX, XXX−XXX

Chart 1. Cyclonickelated Species Derived from Aryl Phosphinites

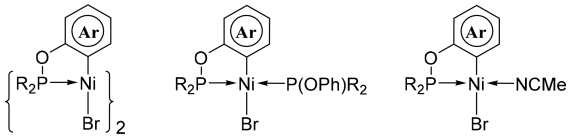

studies: they are derived from phenols, which are inexpensive and ubiquitous in organic synthesis; the PR_2 directing group is easily grafted onto phenols by reaction with $ClPR_2$; ^{31}P NMR spectroscopy provides a convenient and powerful method for monitoring reactions and detecting intermediates. These advantages compelled us to undertake detailed mechanistic studies on C−H cyclonickelation of aryl phosphinites. In a recent report,[9] we presented an optimized synthetic protocol for the preparation of cyclonickelated complexes shown in Chart 1 and provided a detailed analysis of the electronic and steric effect of phenol substituents on cyclonickelation rates, regiochemistry, and solid-state structures of the cyclonickelated complexes.

The present contribution reports on our continued investigations of the reactivities of Ni(II) precursors with aryl phosphinites. The focus of this report is identification of the in situ generated Ni species that promote the C−H nickelation step. Our investigation of the reaction conditions affecting the rate of this step has revealed a crucial role for the solvent, as well as the type and quantity of amine bases used. Deuterium labeling experiments have revealed that the C−H/C−D nickelation step occurs in the absence of base, but *isolation* of the cyclonickelated product arising from this reaction requires a relatively strong base. Kinetic studies and a Hammett analysis have provided quantitative data about the rate and nature of the C−H nickelation step. Finally, DFT studies have supported the mechanistic insights obtained from experimental studies.

RESULTS AND DISCUSSION

Effect of Solvent on Cyclonickelation. We have reported previously that ortho-C−H nickelation of aryl phosphinites is faster in acetonitrile relative to toluene, THF, and EtOAc.[10] Initially, we attributed this observation to the greater ability of a polar solvent such as acetonitrile for stabilizing the nickelation transition state, which is believed to involve significant charge separation over the reacting moieties $C^{\delta-}$- - -$H^{\delta+}$ and $Ni^{\delta+}$- - -$Br^{\delta-}$.[10] However, on reflection it occurred to us that another reason for the more facile cyclonickelation in acetonitrile might be this solvent's greater nucleophilicity toward Ni(II).[11] Thus, the more favorable MeCN→Ni coordination could conceivably generate a solvent adduct such as (L)(MeCN)$NiBr_2$ (**1a**, L = PhOP(*i*-Pr)$_2$) that would be more reactive toward cyclonickelation relative to the biphosphinite complex *trans*-L_2NiBr_2 (**1b**) present in toluene.[12]

The assertion that a different intermediate might form in acetonitrile was consistent with the observation of differently colored initial reaction mixtures as a function of solvent. For instance, stirring the insoluble Ni precursor $[(i\text{-PrCN})NiBr_2]_n$ in toluene solutions of PhOP(*i*-Pr)$_2$ at room temperature generates the toluene-soluble biphosphinite adduct **1b**. The deep red color of this complex dominates the heterogeneous mixture that forms in the presence of less than 2 equiv of L, whereas a homogeneous deep red solution is observed with 2 equiv or more of L. In other words, the L:Ni ratio affects the homogeneity of these toluene mixtures, but not their color. The ^{31}P NMR spectrum of the latter mixtures displayed, independently of the L:Ni ratio, a fairly broad peak spanning the chemical shift interval 132−138 ppm, which could be attributed to dynamic exchange. Recording the ^{31}P spectrum at −30 °C gave significant peak sharpening (Figure S15), and displayed a major peak at 135 ppm, along with a minor peak at 130 ppm which can be attributed to a different conformer of **1b** (i.e., C_2 symmetric vs centrosymmetric).

Repeating the above experiment in acetonitrile revealed two different color regimes depending on the L:Ni ratio. Thus, addition of 1 equiv of phosphinite to the acetonitrile suspension of $[(i\text{-PrCN})NiBr_2]_n$ gave a homogeneous green solution displaying no ^{31}P signal at all, whereas adding another 1 equiv of L led to a deep red solution displaying a very broad ^{31}P signal spanning the chemical shift range of 120−150 ppm. This latter signal was confirmed to be due to **1b** by recording the ^{31}P NMR spectrum of an authentic sample of this compound in acetonitrile. Recording the ^{31}P spectrum of **1b** at −30 °C revealed sharp peaks at 135 ppm (major) and 130 ppm (minor), as well as a peak at 150 ppm corresponding to the free ligand. This indicates that MeCN is nucleophilic enough to allow displacement of the phosphinite and that lowering the temperature slows the exchange process sufficiently to allow us to detect the species involved in the exchange (Figure S16). Moreover, when the green 1:1 L:Ni mixture was subjected to the same analysis, the only detectable peaks were at 135 ppm (major) and 130 ppm (minor, Figure S17); this implies that **1b** also exchanges with the

Scheme 1. Different Ni Species Postulated To Exist in Toluene and Acetonitrile Prior to the Nickelation of PhOP(*i*-Pr)$_2$

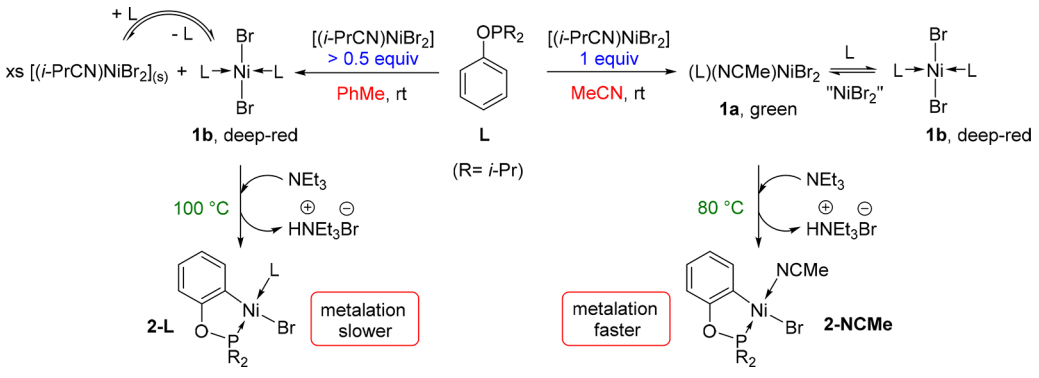

DOI: 10.1021/acs.organomet.8b00899
Organometallics XXXX, XXX, XXX−XXX

biphosphinite species, even though the latter is present to a significantly smaller extent in MeCN than in nonpolar solvents.

The above observations allow us to propose the sequence of events shown in Scheme 1 for rationalizing how PhOP(*i*-Pr)$_2$ and [(*i*-PrCN)NiBr$_2$]$_n$ interact prior to the cyclonickelation stage. We believe that dynamic equilibria are taking place in both solvents at room temperature. In toluene, these equilibria always favor the deep red biphosphinite species **1b**, whereas in acetonitrile it is the green monophosphinite adduct **1a** that is dominant in the presence of 1 equiv of phosphinite. The stability of the monophosphinite species **1a** is presumably due to the nucleophilic character of acetonitrile, whereas related monophosphinite intermediates do not appear to be stable in toluene, THF, or EtOAc.[13] Furthermore, given the broadness of the ^{1}H and ^{31}P signals for the acetonitrile solutions of **1b**, it is reasonable to infer that the competitive binding of the solvent could lead to exchange between bi- and monophosphinite species and that the latter would exist as a paramagnetic tetrahedral form.

Having established that room-temperature reaction mixtures contain different Ni−phosphinite species **1a** and **1b** depending on the solvent and L:Ni ratio, we proceeded to measure how easily each of these species undergoes cyclonickelation. Thus, heating a 1:1:1 L:Ni:Et$_3$N mixture in acetonitrile at 80 °C gave complete cyclonickelation in 16 h, whereas only 50% conversion was observed in toluene under analogous conditions; even heating the toluene mixture to 100 °C gave only 75% conversion.[14] A similar result was obtained when we measured the cyclonickelation rates in the presence of a 2:1 L:Ni ratio. Indeed, heating 1:1 solutions of **1b**:Et$_3$N at 80 °C for 16 h showed complete cyclonickelation in acetonitrile, but only 40% in toluene; the latter mixture required heating to ca. 100 °C to achieve ca. 90% conversion.[15] It appears, therefore, that cyclonickelation is faster in acetonitrile likely because of the reactive monophosphinite intermediate **1a** formed in this solvent (Scheme 1). Conversely, metalation is slower in toluene because the predominant species in this solvent is the biphosphinite complex **1b**; the latter is less reactive since it requires the dissociation of one phosphinite to promote the C−H nickelation. This scenario is also consistent with the observation that the presence of excess L slows the cyclonickelation reaction.[8]

Role and Influence of Base on C−H Nickelation. Our previous studies had shown that the presence of Et$_3$N is essential for successful cyclonickelation of aryl phosphinites; this was attributed to the quenching of the in situ generated HBr.[8,9] However, a more careful analysis of the reaction mixtures prior to cyclonickelation (i.e., prior to heating) gave indications that Et$_3$N might hinder the desired reaction. Thus, although the 1:1 L:Ni mixture in MeCN gives a green solution that is NMR-silent, addition of 1 equiv of Et$_3$N to this solution turned it brownish and gave a broad ^{31}P signal (ca. 120−150 ppm) characteristic of biphosphinite complex **1b** in acetonitrile. We also detected a sharp and minor peak (<2%) on top of the initial broad peak at ca. 135 ppm, but we were unable to identify the species responsible for this resonance. Addition of 3 equiv more of Et$_3$N led to a small amount of free phosphinite (151 ppm), suggesting that competitive binding of the base would hinder the reaction.

To confirm that the observed changes result from the coordination of the base to Ni, we added 1 equiv of the bulkier and less nucleophilic amine *i*-Pr$_2$NEt (Hünig's base) to a green 1:1 L:Ni mixture in acetonitrile. This mixture showed no color change, and its ^{31}P NMR spectrum displayed only the very minor sharp peak at 135 ppm, but not the broad signal at ca. 120−150 ppm attributed to **1b**.

The above observations imply that the NMR-silent feature of the 1:1 L:Ni acetonitrile mixture as well as its green color can be reasonably ascribed to the formation of a paramagnetic tetrahedral monophosphinite adduct such as **1a**. Alternatively, the absence of NMR signals could also indicate a dynamic exchange process, for instance involving various mono- and biphosphinite adducts. Regardless of which interpretation is more probable, addition of a sufficiently nucleophilic amine such as Et$_3$N can lead to a competition for binding to Ni, thus reducing the effective concentration of Ni available for interaction with the phosphinite. In other words, Et$_3$N leads to an effective L:Ni ratio greater than 1:1, thereby leading to the formation of **1b**, which is known to hinder the cyclonickelation reaction. We conclude, therefore, that although Et$_3$N is necessary for driving the reaction to completion by capturing the in situ generated HBr, it also retards the cyclonickelation by promoting the formation of **1b**.

The seemingly counteracting roles of Et$_3$N prompted us to conduct kinetic studies aimed at measuring the effect of [amine] on cyclonickelation of PhOP(*i*-Pr)$_2$. The conversion vs time plots revealed that the C−H nickelation of PhOP(*i*-Pr)$_2$ is faster with 1 equiv of Et$_3$N than with 4 equiv (Figure S38). Plotting ln(1 − conv.) vs time over the first 3 h of the reaction produced fairly straight lines (Figure 1), revealing that

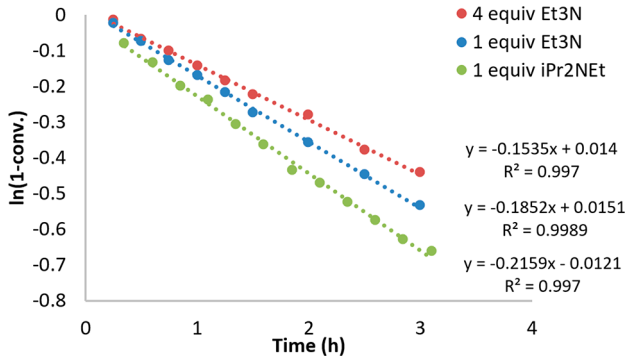

Figure 1. Plot of ln(1 − conv.) as a function of time and rate constants under the assumption of a first-order cyclonickelation in MeCN at 70 °C with various amines and [amine].

the C−H nickelation follows approximately first order rates. The regression gave rate constants of 0.19 and 0.15 h^{-1}, respectively, implying a smaller than zeroth order for the base. This finding is consistent with the aforementioned proposal that competitive Et$_3$N→Ni coordination can diminish the concentration of the species responsible for the C−H nickelation. Moreover, when 1 equiv of base was used, the reaction was faster with *i*-Pr$_2$NEt relative to Et$_3$N (0.22 vs 0.19 h^{-1}), which is also consistent with the diminished inhibitory effect of a more hindered amine on the cyclonickelation.

To further investigate the effect of external base on cyclonickelation, we studied the reaction of [(*i*-PrCN)NiBr$_2$]$_n$ with PhOP(*i*-Pr)$_2$ in the presence of other amines. This reaction was found to be very sensitive to the specific choice of external base, strong bases of weak nucleophilic character being ideal candidates. Thus, little or no reactivity was observed with amines that are weakly basic (e.g., aniline and *N*,*N*-diethylaniline) or strongly coordinating (e.g., pyridine, imidazole,

DOI: 10.1021/acs.organomet.8b00899
Organometallics XXXX, XXX, XXX−XXX

pyrazole, and DBU). In the case of the latter amines, immediate color changes were observed upon addition of the amine, confirming the competitive coordination of the amine, thus hindering the metalation. These findings can be summed up as follows: external bases can hinder cyclonickelation of aryl phosphinites if they are strongly coordinating and/or present in superstoichiometric amounts; nevertheless, they play an essential role in the fate of cyclonickelation, one that cannot be fulfilled by excess phosphinite, which is insufficiently basic to quench HBr.

Reversibility of the Nickelation. It occurred to us that the requirement for a strong base could be understood if the nickelated complex was easily protonated. In such a scenario, protonation of weak bases (including phosphinites) by the in situ generated HBr would give rise to a strong conjugate acid capable of protonating the newly formed Ni−C bond, thus reversing the nickelation step. Conversely, reaction of strong external bases with HBr would form weak conjugate acids that would not be effective for protonating the Ni−C moiety; this would drive the cyclonickelation forward. To determine the validity of this hypothesis, we tested the stability of the independently prepared and authenticated complexes $[\{\kappa^P,\kappa^C\text{-}C_6H_4OP(i\text{-}Pr)_2\}Ni(\mu\text{-}Br)]_2$ (**2-μBr**) and **2-NCMe** in the presence of a relatively strong proton source, as described below in Scheme 2.

Scheme 2. Protonation of the Aryl Moiety by AcOH

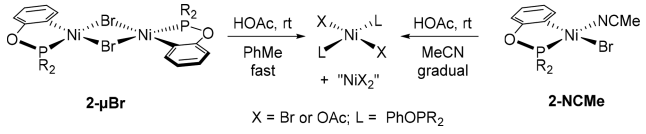

Addition of 1 equiv of acetic acid to the room-temperature acetonitrile solution of **2-NCMe** caused a gradual color change to a deeper red, and the original ^{31}P signal at 196 ppm was partially replaced over a few hours by a broad signal at ca. 135 ppm; this is the signal for the nonmetalated complexes *trans*-L_2NiX_2 (X = Br, OAc). A similar reactivity was observed when 2 equiv of acetic acid was added to the toluene solution of **2-μBr** at room temperature, but in this case the color change took place in the time of mixing, and the ^{31}P NMR spectrum recorded within 10 min confirmed complete disappearance of the starting material. These observations indicate that the C−H nickelation of aryl phosphinites is reversible even in the presence of a relatively weak organic acid. Moreover, tests also showed that the phosphinite could not be protonated in the presence of acetic acid or an even stronger acid such as 3-Cl-C_6H_4COOH, demonstrating that the conjugate acid $[i\text{-}Pr_2P(H)OPh]^+$ must be a sufficiently strong acid to reverse the cyclonickelation step.

The above results indicate that the cyclonickelated complex is thermodynamically unstable toward reprotonation by HBr, but it should be kinetically accessible even in the absence of a base. To prove this, we sought evidence for H/D scrambling between a phosphinite and its deuterated analogue under the conditions of C−H nickelation; if the cyclonickelated species arising from these phosphinites could survive in the medium long enough, the ensuing reprotonation by HBr/DBr should leave a trace of the cyclonickelation event.

The above hypothesis was tested by refluxing a 1:1 mixture of *trans*-$(C_6D_5OPR_2)_2NiBr_2$ (R = *i*-Pr, **1b-d$_5$**) and *trans*-(4-Cl-$C_6H_4OPR_2)_2NiBr_2$ (**1b-Cl**) in d_0-acetonitrile over 24 h in the absence of added base (Scheme 3). The nickel complexes present in the final reaction mixture were isolated by crystallization and analyzed by ^1H NMR in $CDCl_3$, which showed H incorporation into the ortho position of the deuterated ligand but none into meta/para positions. Surprisingly, however, there was no significant decrease in the ^1H signal for the ortho H in **1b-Cl**, indicating that this compound was not the source of the protons incorporated into **1b-d$_5$**. This raised the question of whether the H/D scrambling occurs with the solvent. In such a scenario, scrambling of phosphinite ortho positions with CH_3CN would occur for both complexes but would be detectable only in the deuterated ligand.

To test this second hypothesis, we refluxed the deuterated complex **1b-d$_5$** alone in CH_3CN for 24 h and analyzed the final product as above, which showed that the ligand had incorporated 17% H into only the ortho positions (Scheme 4). However, $^2H\{^1H\}$ NMR of the sample in $CHCl_3$ revealed

Scheme 4. Proposed Mechanism for the Role of Solvent in the Incorporation of H into Deuterio Ligand

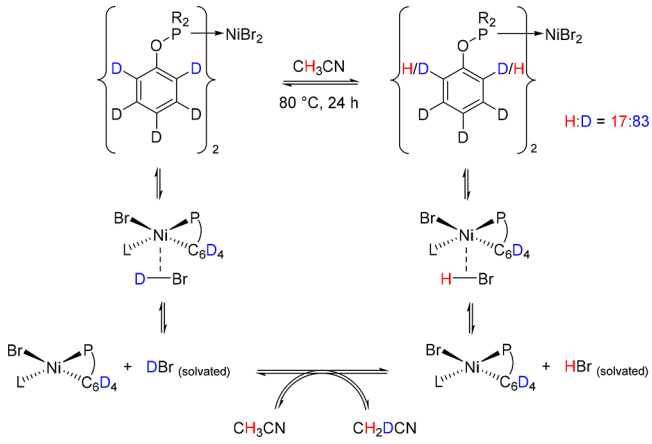

signals corresponding to ortho D in the ligand above natural abundance. Although the signal was too small to be accurately quantified, comparison with the natural abundance of $CDCl_3$ in $CHCl_3$ allowed us to evaluate that the extent of D incorporation is well below 1% (Figure S29). These results can

Scheme 3. Observed Ortho H/D Scrambling between Complexes 1b-d$_5$ and 1b-Cl in MeCN

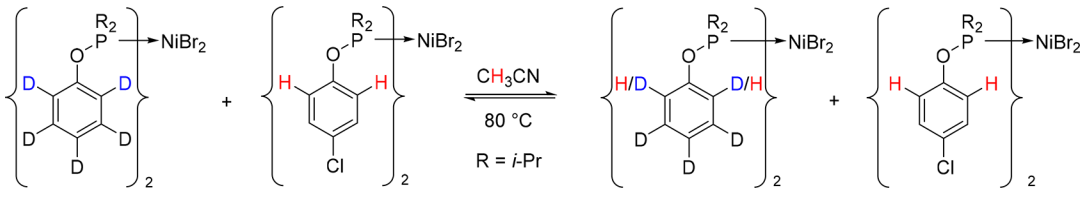

DOI: 10.1021/acs.organomet.8b00899
Organometallics XXXX, XXX, XXX−XXX

be rationalized by invoking H/D exchange between the in situ generated DBr and the reaction solvent to generate HBr (eq 1). The HBr will then protonate the newly formed Ni−C bond (eq 2), thus accounting for H incorporation into **1b-d$_5$** (Scheme 4). We should note as well that $^{13}C\{^1H\}$ NMR analysis of the final material (Figures S32 and S33) showed that the *i*-Pr moieties of the ligand have not incorporated any D, as we detected no signal for *C*DMe$_2$ or CHMe (*C*DH$_2$); this confirms that the H/D exchange takes place with the solvent. This sequence of reactions takes place because the H/D exchange between the in situ generated DBr and CH_3CN (eq 1) proceeds with a rate that is similar to the protonation of the newly formed C−Ni bond by the HBr generated in the exchange (eq 2). In contrast, the analogous H/D exchange between **1b** and CD_3CN is not observed, probably because the H/D exchange in CD_3CN (eq 3) is slower than the protonation of the C−Ni bond (eq 2).

$$CH_3CN + DBr \rightleftharpoons CH_3CND^+ + Br^- \rightleftharpoons CH_2DCNH^+ + Br^- \rightleftharpoons CH_2DCN + HBr \quad (1)$$

$$HBr + \textbf{2-L} \rightarrow \textbf{1b} \quad \text{fast} \quad (2)$$

$$CD_3CN + HBr \rightleftharpoons CD_2HCN + DBr \quad \text{slow} \quad (3)$$

Repeating the above experiments in toluene gave similar results. Heating **1b-d$_5$** in the absence of a base for 24 h at 100 °C in d_0-toluene showed 23% H incorporation into the ortho position of the ligand under the same conditions (and no D incorporation into the *i*-Pr moieties); moreover, $^2H\{^1H\}$ NMR did not show ortho D incorporation into the ligand, suggesting this to be below the detection limit (<0.1%). In this case, the H/D exchange between in situ generated DBr and toluene is conceivably going through a protonated arene such as a Wheland intermediate (eq 4).

$$C_6H_5CH_3 + DBr \rightleftharpoons [C_6H_5(D)CH_3]^+ + Br^- \rightleftharpoons C_6H_4DCH_3 + HBr \quad (4)$$

As was discussed for the analogous reactivity in CD_3CN, no H/D exchange is observed in d_8-toluene owing to slow exchange with this solvent. Although the nickelation is known to be slower in toluene than in acetonitrile, more H incorporation has been observed in toluene (23% vs 17%); this indicates that the exchange of DBr with toluene is faster than that with acetonitrile and that the rate-limiting step in acetonitrile is this exchange, and not the nickelation step.

Altogether, the results of the D/H exchange experiments described above confirm that the C−H nickelation of aryl phosphinite can take place in the absence of an external base. Significantly, these observations also imply that capture of the acid formed in the immediate aftermath of the C−H nickelation step by the base takes place outside the coordination sphere.

Kinetics of Aryl Phosphinite Cyclonickelation. The observations described in the above sections established that the most favorable conditions for cyclonickelation of aryl phosphinites are the following: running the reactions in acetonitrile with the phosphinite ligand, our Ni precursor, and *i*-Pr$_2$NEt in a 1:1:1 ratio. Monitoring the reaction under these conditions at 80 °C and plotting ln(1 − conv.) against time revealed first-order kinetics for the cyclonickelation up to 90% conversion, although a somewhat faster rate is evident at the beginning of the reaction (Figure 2). The observed first-order C−H nickelation is consistent with the previously stated proposal that the base plays no role in the rate-determining step.

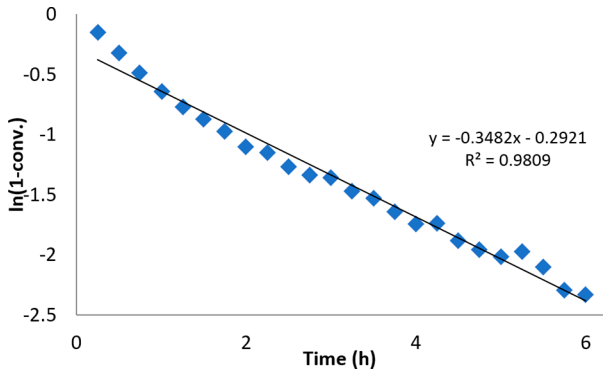

Figure 2. Plot of ln(1 − conv.) as a function of time for the cyclonickelation of PhOP(*i*-Pr)$_2$ with 1 equiv of Ni precursor and 1 equiv of *i*-Pr$_2$NEt in MeCN at 80 °C.

In an effort to shed some light on the possible reaction pathways, we conducted a Hammett analysis on the cyclonickelation of substituted aryl phosphinites. Monitoring the cyclonickelation of various meta-substituted aryl phosphinites 3-X-C$_6$H$_5$OP(*i*-Pr)$_2$ (X = COOMe, Cl, H, Me, OMe) at 80 °C revealed a strong dependence on the electron-withdrawing (EW) or electron-donating (ED) character of the substituent (Figure 3). Indeed, the Hammett plot displays a strongly

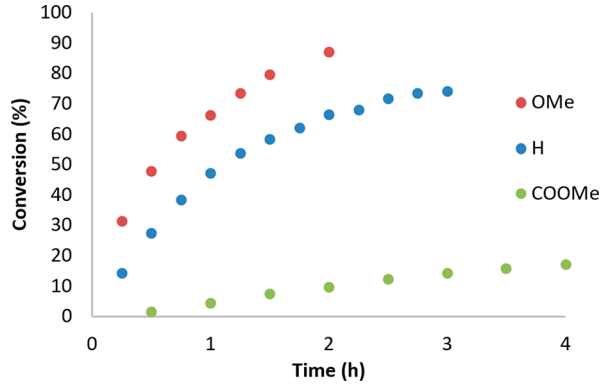

Figure 3. Nickelation rates of various 3-X-C$_6$H$_5$OP(*i*-Pr)$_2$ species in MeCN at 80 °C.

negative slope ($\rho \approx -4$, Figure 4), indicating a much faster C−H nickelation rate for substrates bearing ED substituents.The fastest rate, obtained for the cyclonickelation of 3-MeO-C$_6$H$_4$OP(*i*-Pr)$_2$, is ca. 20 times greater than the slowest rate, obtained for the cyclonickelation of 3-COOMe-C$_6$H$_4$OP(*i*-Pr)$_2$. Consistent with these results, cyclonickelation of the highly electron rich substrate 3-Me$_2$N-C$_6$H$_4$OP(*i*-Pr)$_2$ proved too fast to be measured conveniently at 80 °C (>70% conversion within 15 min); indeed, this reaction proceeded to completion even at room temperature, over 16 h. Finally, the cyclometalation of sterically hindered 3,5-(MeO)$_2$-C$_6$H$_5$)OP(*i*-Pr)$_2$ was found to be faster than the analogous reaction with the unsubstituted PhOP(*i*-Pr)$_2$ (Figure S41), demonstrating that favorable electronic factors can overcome unfavorable steric effects.

DOI: 10.1021/acs.organomet.8b00899
Organometallics XXXX, XXX, XXX−XXX

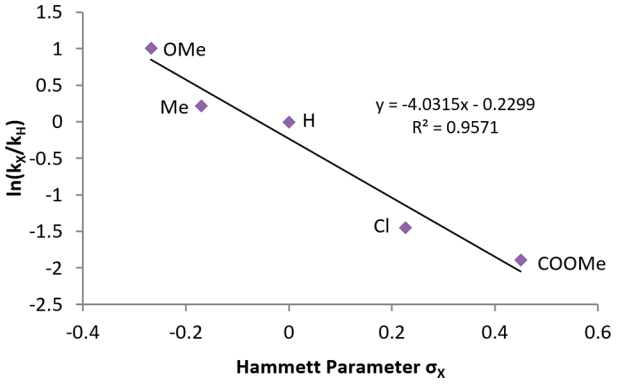

Figure 4. Hammett plot for the nickelation of 3-X-$C_6H_5OP(i\text{-}Pr)_2$ species in MeCN at 80 °C.

The favorable impact of ED substituents on cyclonickelation of aryl phosphinites indicates that a positive charge develops on the Ni center at the transition state, which is stabilized by the coordination of the C−H moiety. This argues in favor of an electrophilic C−H metalation. To determine the importance of the proton transfer on the overall C−H nickelation rate, we examined the relative reaction rates for the cyclonickelation of $C_6H_5OP(i\text{-}Pr)_2$ and its deuterio analogue $C_6D_5OP(i\text{-}Pr)_2$. The reaction with the latter was much slower, and we observed $k_H/k_D \approx 11$ (Figure S42). The large value for the kinetic isotope effect suggests that the proton transfer is the rate limiting step in the mechanism.

Next, we studied metalation rates of $PhOP(i\text{-}Pr)_2$ between 50 and 80 °C. The linear regression of the Eyring plot (Figure 5) allowed us to extract the idealized kinetic parameters

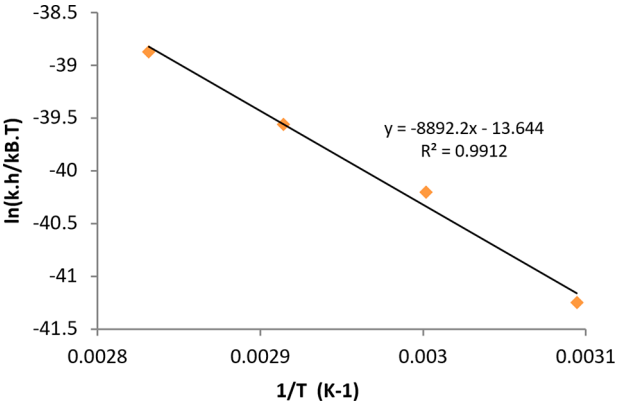

Figure 5. Eyring plot displaying rates at 50, 60, 70, and 80 °C for the metalation of $PhOP(i\text{-}Pr)_2$ in MeCN.

according to the transition state theory: $\Delta H^{\ddagger} = 17.7$ kcal mol^{-1} and $\Delta S^{\ddagger} = -27.1$ cal mol^{-1} K^{-1}. The large and negative $\Delta S^{\ddagger}$ suggests a rate-limiting step with fewer degrees of freedom: i.e., a highly ordered transition state. This finding implies that the pathway from the resting state of the active species to the transition state for C−H nickelation must involve association as opposed to dissociation.

Attempts To Isolate Reaction Intermediates in Acetonitrile. *Identification of Et_3N→Ni Intermediates.* The aforementioned findings on the formation of the less reactive biphosphinite complex **1b** being favored in the presence of excess Et_3N prompted us to probe how binding of Et_3N to Ni can impact the latter's reactivity with aryl phosphinites. To do so, we set out to isolate Et_3N→Ni adducts in the absence of the phosphinite, as follows.

Adding 2 equiv of Et_3N to a green suspension of $[(i\text{-}PrCN)NiBr_2]_n$ in acetonitrile caused an instantaneous color change to deep blue and rendered the mixture homogeneous; addition of Et_2O and cooling to −35 °C for a few hours yielded large royal blue crystals. Exposing these crystals to ambient air for even a few seconds led to formation of a green crust on the crystal, presumably hydrates. Crystallographic analysis of the material proved challenging due to significant decomposition during crystal mounting and data collection; nevertheless, the collected data allowed us to unambiguously identify the main blue species as the homonuclear salt $[Ni(NCMe)_6][(Et_3N)NiBr_3]_2$ (Scheme 5).

Scheme 5. Isolation of Et_3N Adducts of Ni

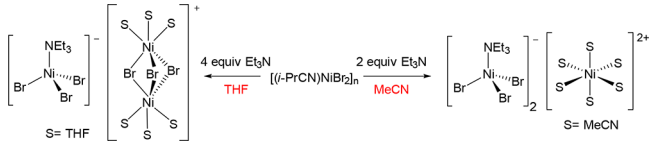

To determine if new, acetonitrile-free species could form in the presence of Et_3N, we repeated the above experiment in the less nucleophilic solvent THF. Adding 4 equiv of Et_3N to $[(i\text{-}PrCN)NiBr_2]_n$ in THF at room temperature also gave a blue solution that yielded blue crystals upon addition of Et_2O and cooling to −35 °C. Analysis of these crystals revealed the formation of another homonuclear salt featuring the same anion, $[(Et_3N)NiBr_3]^-$, but a different cationic species, namely the μ-Br bridged dinuclear adduct of THF (Scheme 5 and Figure 6). It appears, therefore, that formation of the

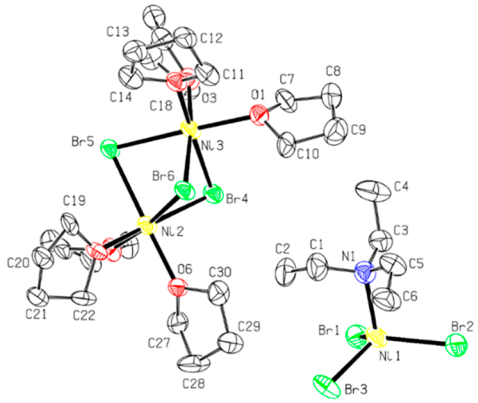

Figure 6. Molecular diagram of $[(THF)_6Ni_2(\mu\text{-}Br)_3]$-$[(Et_3N)NiBr_3]$. Thermal ellipsoids are shown at the 50% probability level. Hydrogens atoms have been omitted for clarity.

tetrahedral anion $[(Et_3N)NiBr_3]^-$ is strongly favored and that this species serves to divert some of the Ni (in a reversible manner) from the main path of the cyclonickelation reaction. This finding allows us to propose the scenario depicted in Scheme 6 for the speciation of Ni in the initial stages of the cyclonickelation.

Isolation of a Proposed Monophosphinite Intermediate. In an effort to isolate the cyclonickelation-active monophosphinite species depicted in Scheme 6, we stirred an equimolar acetonitrile solution of $[(i\text{-}PrCN)NiBr_2]_n$ (ca. 0.1 M) and $PhOP(i\text{-}Pr)_2$ and cooled the resulting green mixture to

DOI: 10.1021/acs.organomet.8b00899
Organometallics XXXX, XXX, XXX−XXX

Scheme 6. Postulated Mechanism of Action of Et_3N in Slowing Cyclonickelation in MeCN

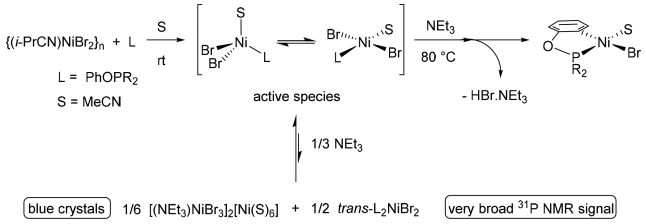

−35 °C. This gave deep red crystals of the biphosphinite complex **1b** and green-yellow crystals that were identified as the coordination polymer of the formula $[NiBr_2(NCMe)_2]_n$. The failure to isolate the target monophosphinite species is attributed to the propensity of **1b** and $[NiBr_2(NCMe)_2]_n$ to equilibrate readily and also to their limited solubility in acetonitrile at lower temperatures.

In a second effort to isolate the putative monophosphinite adduct, we prepared the parent charge-tagged phosphinite salt $[3\text{-}Me_3N\text{-}C_6H_4OP(i\text{-}Pr)_2]X$, L'^+X^- (X = Cl, I) and repeated the above experiment. To avoid potential complications arising from the presence of different halides, we treated L'^+X^- with 2 equiv of Ag(OTs) (Ts = *p*-Me-$C_6H_4SO_2$) in order to replace Cl^- and I^- anions by the less coordinating tosylate anion. This led to immediate precipitation of a white solid (presumably silver salts), which was filtered off. Subsequent addition of 1 equiv of the Ni precursor to the filtrate and stirring at room temperature led to a green solution that displayed broad ^{31}P NMR signals at 161 ppm (major) and 135 ppm (minor). Allowing this green solution to stand at room temperature gave only colorless crystals that turned out to be the dimeric silver salt $[(L'^+Ag)_2(\mu\text{-}Br)_3]Br$ (Scheme 7; see Figure S36 for a molecular diagram). It is worth emphasizing that the anticipated Ni compound was not isolated even after cooling the green filtrate at −35 °C for several days. Evidently, the greater affinity of the phosphinite for Ag(I) appears to circumvent the isolation of Ni−phosphinite species.

Finally, we treated the in situ generated L'^+X^- directly with 1 equiv of $[(i\text{-PrCN})NiBr_2]_n$ in MeCN at room temperature and analyzed the green solution by ESI-MS. The result was most consistent with the formation of $(MeCN)_n(L'^+)NiBr_2$ species (n = 1, 2).[16] Cooling this solution to −35 °C overnight gave deep green crystals that turned out to be the zwitterionic monophosphinite adduct $\{3\text{-}Me_3N\text{-}C_6H_4OP(i\text{-}Pr)_2)\}NiX_3$ (X = Cl, Br, Scheme 7; see Figure S37 for a molecular diagram).

The unanticipated formation of an anionic trihalide species can be ascribed to the high halide:Ni ratio of 4:1 in this mixture vs the 2:1 ratio present under the usual conditions of cyclonickelation.

In conclusion, our attempts to isolate or detect the putative cyclonickelation intermediate were unsuccessful. Nevertheless, the existence of a reactive, monophopsphinite species in acetonitrile mixtures of the Ni precursor and phosphinites is supported by (a) isolation of the monophopsphinite zwitterionic complex illustrated in Scheme 7 and (b) the fact that this tetrahedral compound has the same color (green) as the species generated in an equimolar solution of $[(i\text{-PrCN})NiBr_2]_n$ and $PhOP(i\text{-Pr})_2$. Further support for the intermediacy of such species in the cyclonickelation process was provided by the DFT calculations presented in the following section.

DFT Computational Analysis. Our DFT calculations started with model compounds based on the simpler phosphinite $PhOPMe_2$. This simplification allowed us to explore a larger range of mechanistic scenarios at a lower computational cost and eventually eliminate the least realistic pathways; subsequent DFT studies were then undertaken with $PhOP(i\text{-Pr})_2$ phosphinites in order to describe our system more accurately. All energies discussed in the following sections for local minima and for transition states are calculated Gibbs free energies.

Ground State. M06 was used to start the optimization of the tetracoordinated, 16-electron model compound $(PhOPMe_2)NiBr_2(NCMe)$, which was allowed to adopt the cis or trans square-planar singlet geometry (^{1}***cis*-1** and ^{1}***trans*-1**) or a tetrahedral triplet geometry (^{1}***tet*-1**). For each of these, we considered as starting points different rotamers (rotation around the Ni−P bond) as well as different orientations for the Ph moiety, pointing away from the Ni center or pointing toward it. In each of the three geometries considered, several local minima were found within a range of 1−2 kcal/mol, with those that featured the Ph group pointing toward the Ni atom being more stable. Taking into account the more stable rotamer found for each geometry (Figure 7), ^{1}***trans*-1** was found to be the most stable, followed closely by ^{3}***tet*-1** (1.0 kcal/mol higher), and ^{1}***cis*-1**, which was significantly less stable (4.7 kcal/mol higher).

For the sake of completeness, we also probed the viability of the pentacoordinated 18-electron species $(PhOPMe_2)Br_2Ni(NCMe)_2$, optimizing it as a square-pyramidal singlet or a trigonal-bipyramidal (*tbp*) triplet. The first approach led to dissociation of the apical acetonitrile, implying that this option

Scheme 7. Species Obtained from Reactions of a Charge-Tagged Ligand with Ni Precursor

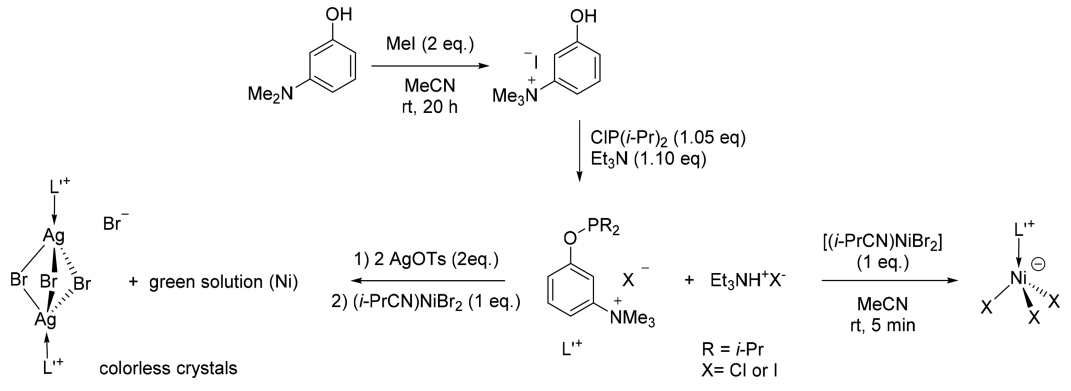

DOI: 10.1021/acs.organomet.8b00899
Organometallics XXXX, XXX, XXX−XXX

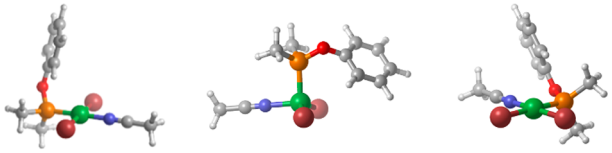

^{1}trans-1	^{3}*tet*-1	^{1}*cis*-1
0.0	+ 1.0	+ 4.7

Figure 7. Energies (calculated at the M06 level of theory and expressed in kcal/mol) for optimized structures of the potential ground states for the model compound $(PhOPMe_2)NiBr_2(NCMe)$.

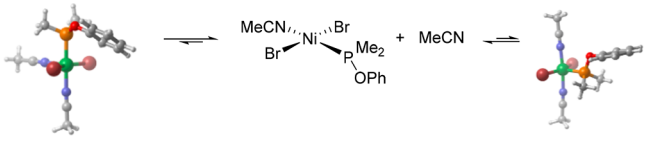

^{3}*tbp*-1-ax	^{1}*trans*-1 + MeCN	^{3}*tbp*-1-eq
+ 6.7		+ 6.6

Figure 8. Energies (calculated at the M06 level of theory and expressed in kcal/mol) for optimized structures as the potential ground states for the pentacoordinated model compound $(PhOPMe_2)NiBr_2(NCMe)_2$.

is unlikely (Figure 8). The second approach led to two distinct options featuring equatorial Br ligands and the phosphinite occupying either an equatorial (**^{3}*tbp*-1-eq**) or an axial position (**^{3}*tbp*-1-ax**). Both of these species proved to be less stable (by ca. 7 kcal/mol) with respect to **^{1}*trans*-1**, implying that the latter four-coordinated species is the most realistic option.

Optimization of the geometries discussed above with B3LYP led to different conclusions. The ground state was found to be **^{3}*tet*-1**, whereas **^{1}*trans*-1** and **^{1}*cis*-1** were found to be more energetic by 8.3 and 11.6 kcal/mol, respectively. It should be noted here that the much greater stability observed for the triplet tetrahedral isomer likely results from B3LYP's propensity to artificially stabilize high-spin over low-spin states.[17] Finally, the *tbp* geometries were disfavored by more than 11 kcal/mol.

Mechanistic Pathways. In accordance with our experimental data, we tested three plausible mechanistic scenarios: (a) C−H oxidative addition followed by H−Br reductive elimination, (b) concerted σ bond metathesis, and (c) ion-pair-assisted electrophilic C−H deprotonation/metalation. To examine the premises of the first scenario, we evaluated the kinetic accessibility of the Ni(IV) intermediates originating from a C−H bond oxidative addition. The three octahedral species shown in Figure 9 were considered as probable intermediates differing in the relative position of the MeCN relative to the aryl moiety.

All attempts to minimize **^{1}Oxadd-1-m*cis*eq** with M06 converged to its precursor Ni(II) square planar species **^{1}*trans*-1**, suggesting that this species is not viable. Optimization of the species **^{1}Oxadd-1-m*cis*ax** and **^{1}Oxadd-1-m*trans*** did converge to local minima, albeit at very high energies of 43.9 and 48.2 kcal/mol, respectively. The transition states for accessing these intermediates were found quite close in geometry and displayed barriers of 44.6 and 48.5 kcal/mol, respectively. Using B3LYP also gave very high energies for barriers and intermediates (>52 kcal/mol above ground state).

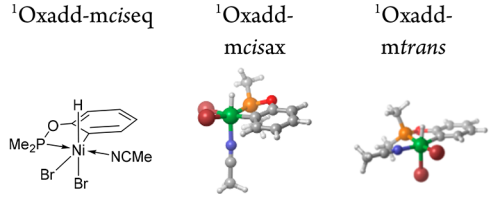

	^{1}Oxadd-m*cis*eq	^{1}Oxadd-m*cis*ax	^{1}Oxadd-m*trans*
E *vs.* GS (barrier)	N/A	43.9 (44.6)	48.2 (48.5)

Figure 9. Energies and kinetic barriers (calculated at the M06 level of theory and expressed in kcal/mol) for the species resulting from C−H oxidative addition.

The very high energies found for the mechanisms involving Ni(IV) species thus rule out scenario a.

Next, we considered scenario b. Proceeding with M06 in the search for a transition state for the concerted σ bond metathesis always led to a transition state for the ion-pair-assisted deprotonation, implying that scenario b is also unlikely. In contrast, the search for an ion-pair-assisted deprotonation (scenario c) led to proton transfer transition states for each of the precursor geometries **^{1}*trans***, **^{1}*cis***, and **^{3}*tet*** (Figure 10). The energy barriers found with M06 were 26.4

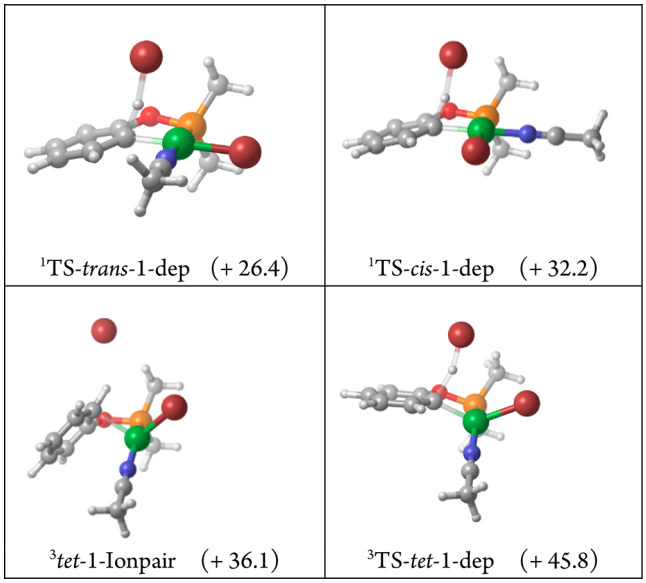

Figure 10. Energies (calculated at the M06 level of theory and expressed in kcal/mol) of the optimized transition states for the deprotonation on the **^{1}*cis***, **^{1}*trans*** and **^{3}*tet*** surfaces as well as the ion pair on the triplet surface.

kcal/mol for **^{1}TS-*trans*-dep** and 32.2 kcal/mol for **^{1}TS-*cis*-dep**. These transition states were linked by the intrinsic reaction coordinate (IRC) path to the nickelated species and HBr (respectively **^{1}*trans*-2** + HBr and **^{1}*cis*-2** + HBr) and to the nonmetalated complexes (**^{1}*trans*-1** and **^{1}*cis*-1**, respectively), albeit without finding ion pairs as local minima.

Exploration of the ion-pair-assisted deprotonation scenario on the triplet surface gave the following results. A transition state was found for this pathway at a barrier of 45.8 kcal/mol (**^{3}TS-*tet*-1-dep**). The IRC path revealed an ion pair as a local minimum at 36.1 kcal/mol, which can be considered an intermediate (**^{3}*tet*-1-Ionpair**) for the heterolytic dissociation

DOI: 10.1021/acs.organomet.8b00899
Organometallics XXXX, XXX, XXX−XXX

Scheme 8. Proposed Energy Surface for the Nickelation of $PhOPMe_2$[a]

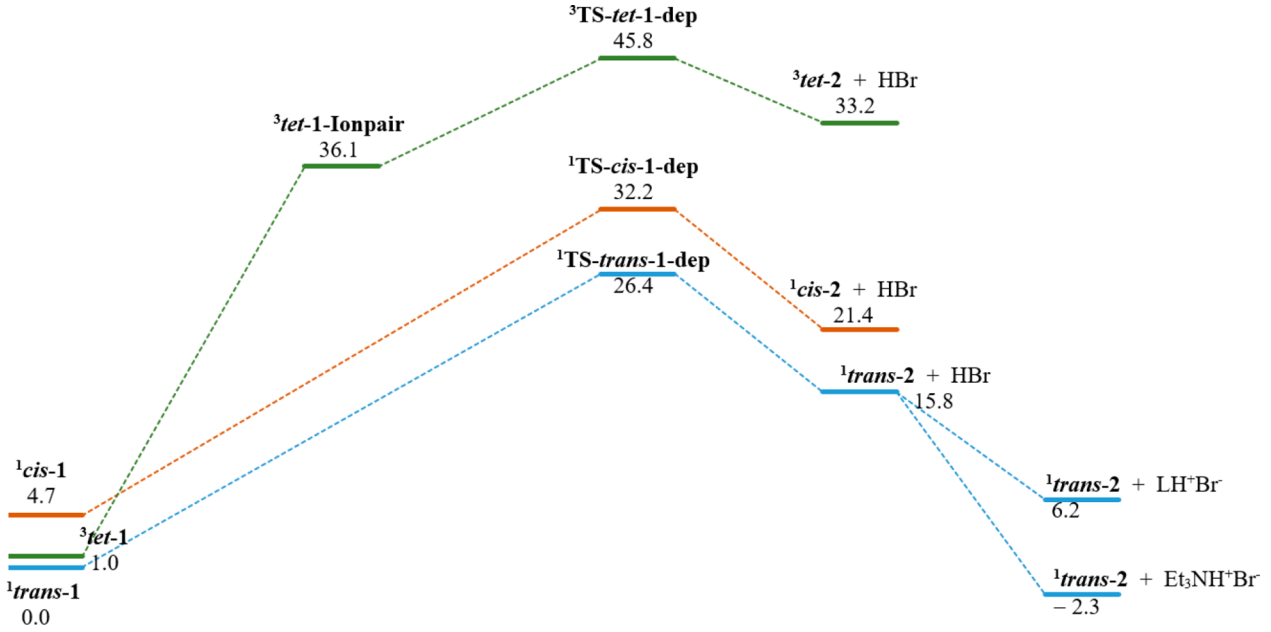

[a]Energies were calculated at the M06 level of theory and are expressed in kcal/mol.

step (leading to the ion pair). Moreover, no transition state was found for the heterolytic dissociation of the bromide ligand, i.e. **^{3}*tet*-1** → **^{3}*tet*-1-Ionpair**, suggesting a TS very close to the ion pair. It is worth emphasizing here that the ion pair on the triplet surface is 5−10 kcal/mol higher in energy than the two deprotonation barriers on the singlet surfaces. Exploring scenario b with B3LYP (Scheme S2) gave transition states on the triplet surface as high as 34.1 kcal/mol for **^{1}TS-*trans*-1-dep** and 39.5 kcal/mol for **^{1}TS-*cis*-1-dep**. The IRC path of the latter provided **^{1}*cis*-1-Ionpair** as a local minimum 36.5 kcal/mol above the ground state; as was the case with M06, no ion pair was found on the **^{1}*trans*** pathway. The deprotonation on the triplet surface going through **^{3}*tet*-1-Ionpair** (32.2 kcal/mol) was, once again, found prohibitive, with **^{3}TS-*tet*-1-dep** being as high as 47.2 kcal/mol. Overall, both M06 and B3LYP favor the ion-pair-assisted deprotonation process on the **^{1}*trans*** pathway.

Thermodynamic Considerations. Scheme 8 summarizes the M06 analysis of the cyclonickelation reaction in acetonitrile leading to **2** + HBr. This was found to be an endergonic process with the following ΔG values (in kcal/mol with respect to **^{1}*trans*-1**): **^{1}*trans*-2** + HBr, 15.8; **^{1}*cis*-2** + HBr, 21.4; **^{3}*tet*-2** + HBr, 33.2. The endergonic character of this process echoes the need for a sufficiently strong base to quench the in situ generated HBr and driving the C−H nickelation to completion. Given the Gibbs free energy of 18.1 kcal/mol for the experimental ΔG for protonation of Et_3N by HBr in acetonitrile,[18] we can conclude that this is an effective base for rendering the overall C−H nickelation process exergonic by 2.3 kcal/mol. This accounts for the feasibility of the nickelation in the presence of Et_3N. In contrast, the value of −9.7 kcal/mol we obtained by DFT calculation of the ΔG value for phosphinite protonation by HBr would be insufficient (by ca. 6 kcal/mol) for rendering the overall nickelation exergonic.

The ΔG values of the nickelation process computed using B3LYP revealed the same trend as above (in kcal/mol with respect to **^{3}*tet*-2**): **^{1}*trans*-2** + HBr, 21.7; **^{1}*cis*-2** + HBr, 25.2; **^{3}*tet*-2** + HBr, 31.3 kcal/mol. However, in this case the process is more endergonic, such that nickelation would not proceed even in the presence of Et_3N. We infer here that the thermodynamics is biased by the overstabilized **^{3}*tet*-1**.

Reaction Surface with P Substituents i-Pr. Having completed the analysis of the C−H nickelation pathway with the PMe_2 model, we set out to explore the analogous reaction surface for the $PhOP(i\text{-}Pr)_2$ species. The above results for the PMe_2 model served to guide our study on the $P(i\text{-}Pr)_2$ species. Specifically, we focused on the four-coordinated species only and considered the ion-pair-assisted deprotonation pathway as the most viable reaction mechanism. To prevent falling into local minima defined by various rotamers arising from rotation of the *i*-Pr moieties, we studied the different conformations of these substituents. Among all possible intermediates studied, the more stable conformations were always those that minimize the Me−Me steric interactions, as observed in the crystal structures for $\{ArOP(i\text{-}Pr)_2\}Ni$ complexes.

As was the case with the simplified PMe_2 model, analysis of the ground state with M06 showed that the cis isomer (**^{1}*cis*-iPr-1**) was higher in energy than the trans isomer (**^{1}*trans*-iPr-1**, Figure 11). However, the triplet tetrahedral species (**^{3}*tet*-iPr-1**) is significantly more stable than the square-planar forms

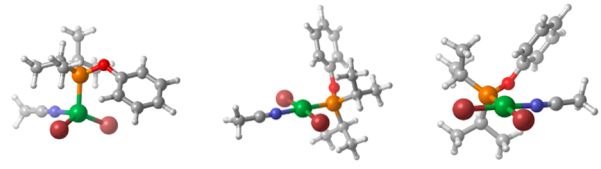

^{3}*tet*-iPr-1 0.0 | ^{1}*trans*-iPr-1 + 3.7 | ^{1}*cis*-iPr-1 + 5.5

Figure 11. Optimized structures for the $\{PhOP(i\text{-}Pr)_2\}NiBr_2(NCMe)$ isomers and their energies calculated at the M06 level of theory. Energies are expressed in kcal/mol.

DOI: 10.1021/acs.organomet.8b00899
Organometallics XXXX, XXX, XXX−XXX

Scheme 9. Proposed Energy Surface for the Nickelation of PhOP(*i*-Pr)$_2$ on ^{1}*trans* and Local Minima on ^{1}*cis* and ^{3}*tet* Pathways[a]

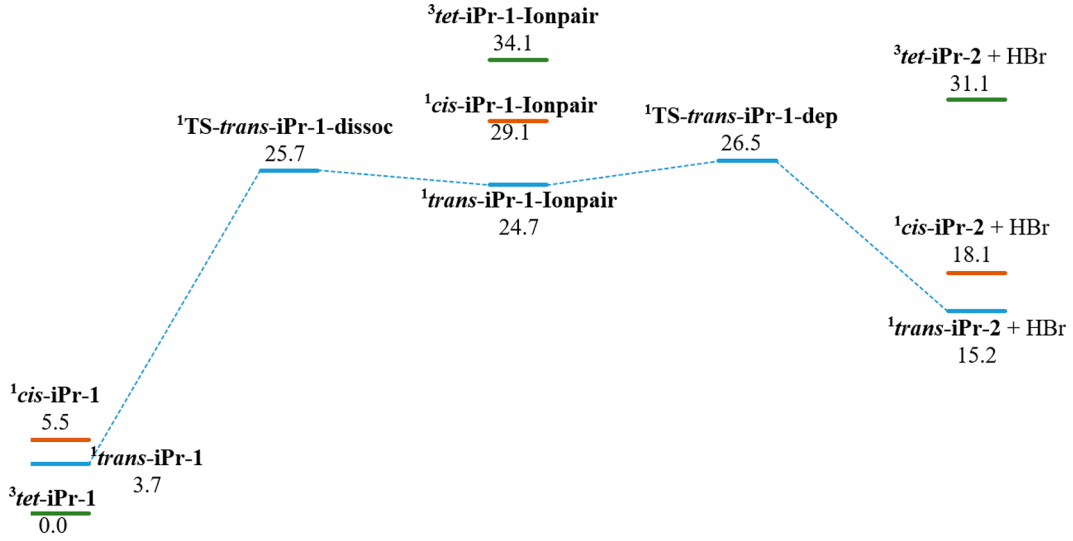

[a]Energies were calculated at the M06 level of theory and are expressed in kcal/mol.

for the P(*i*-Pr)$_2$ system, presumably because of the greater importance of steric demands of the *i*-Pr substituents. This result is also more consistent with the fact that the 1:1 L:Ni mixture is green and NMR-silent, features usually observed for tetrahedral Ni(II) compounds such as the emerald green zwitterionic complex {Me$_3$N-PhOP(*i*-Pr)$_2$}NiX$_3$ (vide supra, Scheme 7). Ion-pair intermediates were found for each of these geometries, with **^{1}*trans*-iPr-1-Ionpair** being the most stable, 24.7 kcal/mol above the ground state, followed by **^{1}*cis*-iPr-1-Ionpair** (29.1 kcal/mol) and **^{3}*tet*-iPr-1-Ionpair** (34.1 kcal/mol).

Analysis of the nickelation thermodynamics gave the following ΔG values for the formation of **iPr-2** + HBr (in kcal/mol with respect to **^{3}*tet*-iPr-2**): **^{1}*trans*-iPr-2** + HBr, 15.2; **^{1}*cis*-iPr-2** + HBr, 18.1; **^{3}*tet*-iPr-2** + HBr, 31.1. Scheme 9 gives a brief analysis of the metalation process for the *i*-Pr species. Thus, conversion of the **^{1}*trans*** isomer to **^{1}*trans*-iPr-1-Ionpair** via Br$^-$ dissociation revealed a transition state at 25.7 kcal/mol, and the deprotonation from the latter ion pair toward the **^{2}*trans*-iPr-2** + HBr went through a slightly higher transition state (26.5 kcal/mol, Figure 12). The ion pairs for the **^{1}*cis*** and **^{3}*tet*** geometries were also found to be higher than **^{1}TS-*trans*-iPr-1-dep**, suggesting that the surface via **^{1}*trans*** is the most probable. Although the strongly negative slope of the Hammett plot is consistent with this pathway, this finding on its own does not allow us to determine if the rate-limiting step is the dissociation or the deprotonation. To settle this question, we resorted to calculating the KIE values associated with different steps to see which would give a KIE value closer to the experimentally determined value.

Frequency calculations on the **^{1}*trans*** surface with the aromatic protons replaced by deuterons allowed us to evaluate the magnitude of the kinetic isotope effect for both dissociation and deprotonation barriers. According to the transition state theory, the k_H/k_D value at 25 °C was found to be 1.2 (1.1 at 80 °C) for the heterolytic Ni−Br dissociation (i.e., the formation of the ion pair) but 8.4 (6.0 at 80 °C) for the deprotonation. The finding that this last step gives a much closer value to the experimentally determined k_H/k_D value of 11 suggests that the rate-limiting step responsible for the observed high KIE is indeed the deprotonation and not the dissociation.

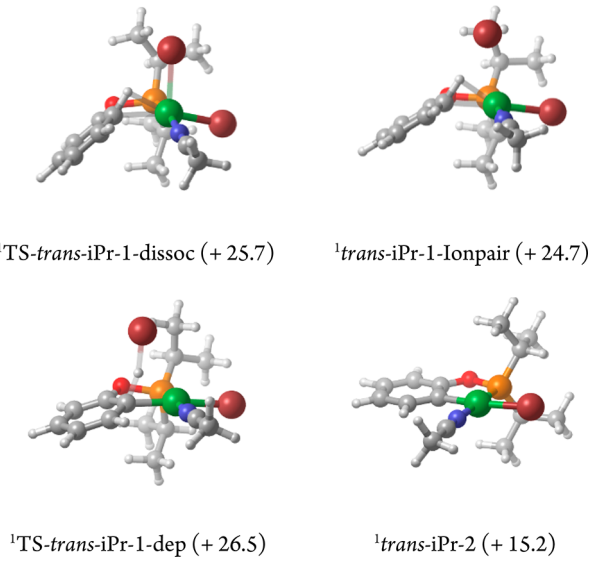

Figure 12. Optimized structures for the P(i-Pr)$_2$ intermediates on the **^{1}*trans*** surface and their energies calculated at the M06 level of theory. Energies are expressed in kcal/mol.

The C−H nickelation process is still endergonic by 15.2 kcal/mol, and the protonation of the ligand PhOP(*i*-Pr)$_2$ by HBr in MeCN was computed to be exergonic by only 9.7 kcal/mol. Therefore, the quenching of HBr by Et$_3$N (−18.1 kcal/mol) is necessary in order to make the overall reaction exergonic by 2.9 kcal/mol. The MECP between the singlet pathways involving **^{1}*trans*/^{1}*cis*-iPr-1** and the triplet surface involving **^{3}*tet*-iPr-1** was not sought, since the experimental observations suggest that the system intercrossing would not be rate limiting in the reaction.

As was the case with the M06 calculations, the metalation reaction analyzed with B3LYP was found to be endergonic, with nickelated adducts **iPr-2** + HBr reaching 18.4, 21.0, and 27.0 kcal/mol above ground state for **^{1}*trans***, **^{1}*cis***, and **^{3}*tet***. The computational analysis with B3LYP also showed that the

DOI: 10.1021/acs.organomet.8b00899
Organometallics XXXX, XXX, XXX−XXX

ground state is ^{3}***tet*-iPr-1**, its stability being greater than those of ^{1}***trans*-iPr-1** (by 9.7 kcal/mol) and ^{1}***cis*-iPr-1** (by 10.6 kcal/mol). The ion pairs for each geometry were shown to follow the same trend as the starting material, with ^{1}***trans*-iPr-1-Ionpair**, ^{1}***cis*-iPr-1-Ionpair**, and ^{3}***tet*-iPr-1-Ionpair** found at 33.0, 34.0, and 27.30 kcal/mol above the ground state, respectively. On the ^{1}***trans*** pathway, the barrier for the dissociation of the bromide to yield the ion pair reached 31.4 kcal/mol and the proton transfer was also found as the rate-limiting step with a barrier of 33.4 kcal/mol. The quenching of HBr by the ligand PhOP(*i*-Pr)$_2$ turned out to be exergonic by only 8.5 kcal/mol. Indeed, these calculations showed that even Et_3N would barely drive the reaction on the ^{1}***trans*** pathway, which reflects the overestimated stability of the high spin ground state with B3LYP

CONCLUSION

This report has established that C−H nickelation of aryl phosphinites is facilitated when this reaction is conducted in acetonitrile and in the presence of an equimolar quantity of NEt_3 or its less nucleophilic homologue *i*-Pr_2NEt. The beneficial role of acetonitrile is believed to originate from the greater nucleophilic character of this solvent (relative to toluene, THF, or EtOAc), which leads to the stabilization of a reactive mono(phosphinite) intermediate. In contrast, the nucleophilic character of a base such as NEt_3 hinders the C−H nickelation by generating various unproductive amine species such as $[(Et_3N)NiBr_3]^-$ and the biphosphinite species $(ArOPR_2)_2NiBr_2$, which is less reactive toward C−H nickelation. DFT calculations have provided support for these conclusions by showing that tetrahedral (and hence NMR-silent) monophosphinite Ni(II) complexes are viable species.

Kinetic studies demonstrated that the C−H nickelation reaction in our system is favored by the presence of electron-donating substituents on the phosphinite aryl ring, thus underlining the importance of the latter's coordination to the electrophilic Ni(II) center. This conclusion is also consistent with the importance of directing groups (the phosphinite moiety in this case) in promoting the C−H nickelation process. The kinetic studies also revealed a very large KIE (~11 at 80 °C), suggesting that C−H bond breaking is rate limiting. A DFT analysis has suggested that the C−H nickelation proceeds through an ion-pair mechanism involving a Ni(II) intermediate.

Another interesting finding touched on the thermodynamics of the C−H nickelation step: H/D exchange studies in deuterio and protio solvents confirmed that C−H nickelation does take place under base-free conditions via an uphill equilibrium, but the newly formed cyclonickelated species is unstable in the absence of a sufficiently strong external base that can quench the in situ generated HBr. The finding that the metalated intermediate is generated in the absence of Et_3N and can survive long enough (before reprotonation) to allow H/D scrambling with the solvent implies that such species are kinetically accessible and should be susceptible to functionalization of the Ni−C moiety in the presence of suitable reagents. This lead will be exploited in our future studies to develop new ortho-functionalization strategies for phenols.

EXPERIMENTAL SECTION

All manipulations were carried out under a nitrogen atmosphere using standard Schlenk techniques and an inert-atmosphere box. Solvents were dried by passage over a column of activated alumina, collected under nitrogen, and stored over 4 Å molecular sieves. Triethylamine was dried over CaH_2. Synthesis of the nickel precursor $[(i\text{-PrCN})NiBr_2]_n$ used throughout this study has been described previously.[19] All other reagents, including deuterated phenol, were purchased from Sigma-Aldrich and used without further purification. All kinetic measurements or studies were conducted by NMR on a Bruker AV400 instrument equipped with a cryoprobe cooled to liquid N_2 temperature. All other NMR spectra were recorded on regular Bruker AV400 or AV500 spectrometers. The C−H nickelation progress was followed by monitoring the ^{31}P NMR signal for $\{\kappa^P,\kappa^C\text{-ArOP}(i\text{-Pr})_2\}Ni(NCMe)Br$ (resonance around 196 ppm in CH_3CN), using $TBAPF_6$ as the internal standard (septet around −150 ppm). The substituted aryl phosphinites were synthesized directly from commercially available phenols and $ClP(i\text{-Pr})_2$ using a reported protocol.[10]

[3-Me$_3$N-C$_6$H$_4$OH]I. 3-*N*,*N*-Dimethylaminophenol (686 mg, 5.0 mmol) was dissolved in 20 mL of CH_3CN to give a deep red solution. MeI (3.11 mL, 50 mmol, 2 equiv) was added slowly and the mixture stirred at room temperature for 20 h, after which a solid formed. A 30 mL portion of Et_2O was added in order to complete precipitation, and the product was filtered, washed with 2 × 15 mL of Et_2O, and dried in vacuo to yield 1.25 g (4.5 mmol, 90%) of a pale purple powder which was found to be pure by ^{1}H NMR in DMSO-d_6.

***trans*-{PhOP(*i*-Pr)$_2$}$_2$NiBr$_2$ (1b).** $PhOP(i\text{-Pr})_2$ (210 mg, 1.0 mmol) was added to a suspension of $[(i\text{-PrCN})NiBr_2]_n$ (287 mg, 1.0 mmol, 1.0 equiv) in 20 mL of Et_2O. The mixture rapidly turned dark red and was stirred at room temperature for 1 h. The excess Ni precursor was removed by cannula filtration, and the residues were extracted twice with 10 mL of Et_2O. Evaporation of the ethereal phase gave 243 mg (0.38 mmol, 76%) of a deep red solid, which was shown to be pure by ^{31}P and ^{1}H NMR in $CDCl_3$. The spectroscopic data in $CDCl_3$ matched literature data.[9] Analytically pure samples were obtained by dissolving the crude compound in a minimum amount of MeCN at room temperature and then cooling to −35 °C for 20 h. The deep red crystals were washed twice with cold acetonitrile (−35 °C) prior to drying under vacuum.

***trans*-{C$_6$D$_5$OP(*i*-Pr)$_2$}$_2$NiBr$_2$ (1b-d$_5$).** This compound was synthesized using the same procedure as described above for **1b**, except for the use of deuterated phenol. The crude powder was directly purified as described above, yielding deep red crystals (330 mg, 0.51 mmol, 51%) . The ^{31}P and ^{1}H NMR spectra in $CDCl_3$ matched those of the related nondeuterated complex, with an absence of the aromatic protons.

***trans*-{4-Cl-C$_6$H$_4$OP(*i*-Pr)$_2$}$_2$NiBr$_2$ (1b-Cl).** This compound was synthesized using the same procedure described above for **1b**, except for the use of 4-Cl-phenol. The crude product (dark red powder) was directly purified as described above for **1b** to give deep red crystals (yield 349 mg, 0.59 mmol, 49%). ^{1}H NMR (500 MHz, 20 °C, $CDCl_3$): δ 1.39 (d, 6H, $CH(CH_3)(CH_3)$, $^3J_{HH}$ = 6.5 Hz), 1.52 (d, 6H, $CH(CH_3)(CH_3)$, $^3J_{HH}$ = 6.6 Hz), 2.75 (sept, 2H, $CH(CH_3)_2$, $^3J_{HH}$ = 7.3 Hz), 7.28 (dm, 2H, C_{ortho}-*H* or C_{meta}-*H*, $^3J_{HH}$ = 8.9, correlated to ^{13}C at δ 129), 7.49 (dm, 2H, C_{ortho}-*H* or C_{meta}-*H*, $^3J_{HH}$ = 8.9 Hz, correlated to ^{13}C δ 121). ^{13}C{^{1}H} NMR (125.7 MHz, 20 °C, $CDCl_3$): δ 18.19 (s, 2C, $CH(CH_3)(CH_3)$), 19.52 (s, 2C, $CH(CH_3)(CH_3)$), 29.76 (s, 2C, $CH(CH_3)(CH_3)$), 121.41 (s, 2C, C_{ortho}-H or C_{meta}-H), 128.01 (s, 1C, *C*-Cl), 129.10 (s, 2C, C_{ortho}-H or C_{meta}-H), 153.64 (s, 1C, *C*-OP). ^{31}P{^{1}H} NMR (202.4 MHz, 20 °C, $CDCl_3$): δ 138 (br s).

H/D Scrambling Attempt between 1b-d$_5$ and 1b-Cl. A Schlenk tube was charged with 100 mg of **1b-Cl**, 100 mg of **1b-d$_5$**, and ca. 2 mL of MeCN. The deep red mixture was heated for 24 h at 80 °C and then cooled to −35 °C for 20 h, leading to the formation of deep red crystals. These were filtered off, washed with 2 × 1.5 mL of cold MeCN (−35 °C), and then dried under vacuum. The crystals were analyzed by ^{1}H NMR analysis in $CDCl_3$ and the spectrum compared to the spectra of approximately equimolar mixtures of crystalline **1b** + **4-Cl-1b** and to equimolar mixtures of crystalline **1b-d$_5$** + **4-Cl-1b**. This comparison confirmed the appearance of only the ortho aromatic protons of **1b** and showed no decrease of the integration for the aromatic protons of **4-Cl-1b**.

DOI: 10.1021/acs.organomet.8b00899
Organometallics XXXX, XXX, XXX−XXX

Protocol for H/D Scrambling with Acetonitrile. A Schlenk tube was charged with 200 mg of the compound (**1b**-d_5 or **1b**) and ca. 2 mL of solvent (CH_3CN or CD_3CN, respectively). The mixture was heated at 80 °C for 24 h and then cooled to −35 °C for 20 h to give crystals, which were isolated, washed twice with 1 mL of cold acetonitrile, dried under vacuum, and analyzed by ^{1}H NMR in $CDCl_3$.

Protocol for H/D Scrambling with Toluene. A Schlenk tube was charged with 200 mg of the compound (**1b**-d_5 or **1b**) and ca. 2 mL of the solvent ($C_6H_5CH_3$ or $C_6D_5CD_3$, respectively). The mixture was heated at 100 °C for 24 h and the solvent evaporated. The residues were redissolved in 2 mL of acetonitrile and cooled to −35 °C for 20 h to give crystals, which were isolated, washed twice with 1 mL of cold acetonitrile, dried under vacuum, and analyzed by ^{1}H NMR in $CDCl_3$.

Protocol for Kinetic Measurements. To a solution of ArOP(*i*-Pr)$_2$ (200 μmol), [(*i*-PrCN)NiBr$_2$]$_n$ (58 mg, 200 μmol, 1.00 equiv), and (*i*-Pr)$_2$NEt (34.8 μL, 200 μmol, 1.00 equiv) in 2.500 mL of MeCN was added a known amount of the standard $TBAPF_6$ (typically 50−100 mg). A 500 μL aliquot of the solution was placed in a J. Young NMR tube. This sample was used for the kinetic measurements by one of the following protocols: (i) the NMR tube was placed in the spectrometer probe and heated to the desired temperature before recording the NMR spectra over the required time interval; (ii) the NMR tube was heated in an oil bath at the desired temperature and for the required time interval before immersing it into a cold-water bath to cool the sample, recording the NMR spectra at room temperature, and repeating the heat−cool−record cycle.

For reactions that went to completion within a reasonable time, the conversion (a number between 0 and 1) at each time t (conv.(t)) was determined by the ratio of integrals in ^{31}P NMR for the metalated species ($A_P(t)$) and the central peak corresponding to PF_6^- ($A_S(t)$), over the same ratio at the end of the reaction (t_{inf}), as follows:

$$\text{conv.}(t) = \frac{A_P(t)}{A_S(t)} \Big/ \frac{A_P(t_{inf})}{A_S(t_{inf})}$$

When the reaction was too slow to reach completion within a reasonable time, conv(t) was determined by the amount of $TBAPF_6$ added, where $A_{S,tot}$ is the total area of the peak for the standard (thus $A_{S,tot} = (64/20)A_S$) and $n_{S,tot}$ the exact amount of $TBAPF_6$ added, in μmol, as follows:

$$\text{conv}(t) = \frac{n_P(t)}{n^0_{substrate}} = \frac{n_P(t)}{200\ \mu\text{mol}} = \frac{1}{200\ \mu\text{mol}} \frac{A_P(t)}{A_{S,tot}(t)} n_{S,tot}$$
$$= \frac{1}{200\ \mu\text{mol}} \frac{A_P(t)}{A_S(t)\frac{64}{20}} n_{S,tot}$$

The first-order rate constants were determined by plotting ln(1 − conv.) vs the time, giving a slope corresponding to $-k$, where k is the rate constant.

Computational Details. The DFT calculations were carried out in implicit MeCN solvent using the SMD model. The basis sets employed for all geometry optimizations and frequency calculations were 6-31g** for light atoms and def2TZVP for Ni and Br, whereas the electronic energy was computed with def2TZVP for all atoms. The optimizations started with the M06 functional,[20] which is known to properly handle ligand−metal bonds and give accurate results on bond dissociation energies.[21] For comparison purposes, the local minima and saddle points were further reoptimized with B3LYP, which is widely used for various DFT computational analyses.[22] High-resolution representations of 3D models were generated by CYLview.[23] Additional computational details as well as the coordinates/energies for all intermediates and transition states are given in the Supporting Information.

■ ASSOCIATED CONTENT

Supporting Information

The Supporting Information is available free of charge on the ACS Publications website at DOI: 10.1021/acs.organomet.8b00899.

NMR spectra, additional plots and figures, and DFT details (PDF)

Accession Codes

CCDC 1865666−1865668 contain the supplementary crystallographic data for this paper. These data can be obtained free of charge via www.ccdc.cam.ac.uk/data_request/cif, or by emailing data_request@ccdc.cam.ac.uk, or by contacting The Cambridge Crystallographic Data Centre, 12 Union Road, Cambridge CB2 1EZ, UK; fax: +44 1223 336033.

■ AUTHOR INFORMATION

Corresponding Author

*E-mail for D.Z.: zargarian.davit@umontreal.ca.

ORCID

Davit Zargarian: 0000-0002-0207-7007

Notes

The authors declare no competing financial interest.

■ ACKNOWLEDGMENTS

The authors gratefully acknowledge financial support provided by the NSERC of Canada (Discovery grants to D. Z.), Centre in Green Chemistry and Catalysis (CGCC/CCVC, summer research stipends and travel awards), and Université de Montréal (graduate scholarships to L. P. M.). We also thank our colleagues from the service laboratories: Dr P. Aguiar (for his availability and help on setting up the ^{31}P NMR kinetic measurements), Sylvie Bilodeau (for VT NMR experiments), Dr. Cédric Malveau (for ^{1}H{^{2}H} experiments), and Dr M. Simard (for help with the resolution of the solid-state structure for complex {Me$_3$N-PhOP(*i*-Pr)$_2$}NiBr$_3$). Finally, we are indebted to Compute Canada-Calcul Canada for access to Westgrid Computational Facilities, and to Mr J.-P. Cloutier for discussions on our DFT studies.

■ REFERENCES

(1) (a) Song, W.; Ackermann, L. Nickel-catalyzed alkyne annulation by anilines: versatile indole synthesis by C−H/N−H functionalization. *Chem. Commun.* **2013**, *49* (59), 6638−6640. (b) Ruan, Z.; Lackner, S.; Ackermann, L. A General Strategy for the Nickel-Catalyzed C−H Alkylation of Anilines. *Angew. Chem., Int. Ed.* **2016**, *55* (9), 3153−3157.

(2) (a) Shiota, H.; Ano, Y.; Aihara, Y.; Fukumoto, Y.; Chatani, N. Nickel-Catalyzed Chelation-Assisted Transformations Involving Ortho C−H Bond Activation: Regioselective Oxidative Cycloaddition of Aromatic Amides to Alkynes. *J. Am. Chem. Soc.* **2011**, *133* (38), 14952−14955. (b) Aihara, Y.; Chatani, N. Nickel-Catalyzed Direct Alkylation of C−H Bonds in Benzamides and Acrylamides with Functionalized Alkyl Halides via Bidentate-Chelation Assistance. *J. Am. Chem. Soc.* **2013**, *135* (14), 5308−5311. (c) Aihara, Y.; Chatani, N. Nickel-Catalyzed Direct Arylation of C(sp3)−H Bonds in Aliphatic Amides via Bidentate-Chelation Assistance. *J. Am. Chem. Soc.* **2014**, *136* (3), 898−901. (d) Aihara, Y.; Tobisu, M.; Fukumoto, Y.; Chatani, N. Ni(II)-Catalyzed Oxidative Coupling between C(sp2)−H in Benzamides and C(sp3)−H in Toluene Derivatives. *J. Am. Chem. Soc.* **2014**, *136* (44), 15509−15512. (e) Song, W.; Lackner, S.; Ackermann, L. Nickel-Catalyzed C-H Alkylations: Direct Secondary Alkylations and Trifluoroethylations of Arenes. *Angew. Chem., Int. Ed.* **2014**, *53* (9), 2477−2480. (f) Wu, X.; Zhao, Y.; Ge, H.

DOI: 10.1021/acs.organomet.8b00899
Organometallics XXXX, XXX, XXX−XXX

Nickel-Catalyzed Site-Selective Alkylation of Unactivated C(sp3)−H Bonds. *J. Am. Chem. Soc.* **2014**, *136* (5), 1789−1792. (g) Landge, V. G.; Shewale, C. H.; Jaiswal, G.; Sahoo, M. K.; Midya, S. P.; Balaraman, E. Nickel-catalyzed direct alkynylation of C(sp2)−H bonds of amides: an "inverse Sonogashira strategy" to ortho-alkynylbenzoic acids. *Catal. Sci. Technol.* **2016**, *6* (6), 1946−1951. (h) Yi, J.; Yang, L.; Xia, C.; Li, F. Nickel-Catalyzed Alkynylation of a C(sp2)−H Bond Directed by an 8-Aminoquinoline Moiety. *J. Org. Chem.* **2015**, *80* (12), 6213−6221. (i) Liu, Y.-J.; Liu, Y.-H.; Yan, S.-Y.; Shi, B.-F. A sustainable and simple catalytic system for direct alkynylation of C(sp2)−H bonds with low nickel loadings. *Chem. Commun.* **2015**, *51* (29), 6388−6391. (j) Yan, S.-Y.; Liu, Y.-J.; Liu, B.; Liu, Y.-H.; Zhang, Z.-Z.; Shi, B.-F. Nickel-catalyzed direct thiolation of unactivated C(sp3)−H bonds with disulfides. *Chem. Commun.* **2015**, *51* (34), 7341−7344. (k) Liu, Y.-H.; Liu, Y.-J.; Yan, S.-Y.; Shi, B.-F. Ni(ii)-catalyzed dehydrative alkynylation of unactivated (hetero)aryl C−H bonds using oxygen: a user-friendly approach. *Chem. Commun.* **2015**, *51* (58), 11650−11653.

(3) Zheng, X.-X.; Du, C.; Zhao, X.-M.; Zhu, X.; Suo, J.-F.; Hao, X.-Q.; Niu, J.-L.; Song, M.-P. Ni(II)-Catalyzed C(sp2)−H Alkynylation/Annulation with Terminal Alkynes under an Oxygen Atmosphere: A One-Pot Approach to 3-Methyleneisoindolin-1-one. *J. Org. Chem.* **2016**, *81* (10), 4002−4011.

(4) See the following report for a rare mechanistic study on this subject: Beattie, D. D.; Grunwald, A. C.; Perse, T.; Schafer, L. L.; Love, J. A. Understanding Ni(II)-Mediated C(sp3)−H Activation: Tertiary Ureas as Model Substrates. *J. Am. Chem. Soc.* **2018**, *140* (39), 12602−12610.

(5) (a) Fontaine, F.-G.; Kadkhodazadeh, T.; Zargarian, D. Nickel indenyl complexes as precatalysts for dehydropolymerization of phenylsilane. *Chem. Commun.* **1998**, No. 12, 1253−1254. (b) Groux, L. F.; Bélanger-Gariépy, F.; Zargarian, D.; Vollmerhaus, R. Preparation and Characterization of Nickel Complexes with η-Indenyl Ligands Bearing a Pendant Aminoalkyl Chain. *Organometallics* **2000**, *19* (8), 1507−1513. (c) Groux, L. F.; Bélanger-Gariépy, F.; Zargarian, D. Phosphino-indenyl complexes of nickel(II). *Can. J. Chem.* **2005**, *83* (6−7), 634−639. (d) Chen, Y.; Sui-Seng, C.; Zargarian, D. Tetraphenylborate as a Novel Bridging Ligand in a Zwitterionic Nickel(I) Dimer. *Angew. Chem., Int. Ed.* **2005**, *44* (47), 7721−7725. (e) Baho, N.; Zargarian, D. Syntheses, Structures, Spectroscopy, and Chromotropism of New Complexes Arising from the Reaction of Nickel(II) Nitrate with Diphenyl(dipyrazolyl)-methane. *Inorg. Chem.* **2007**, *46* (1), 299−308.

(6) For examples of Ni complexes based on various symmetrical or unsymmetrical pincer ligands see the following review and primary reports. (a) Haenel, M. W.; Jakubik, D.; Krüger, C.; Betz, P. 1,8-Bis(diphenylphosphino)anthracene and Metal Complexes1). *Chem. Ber.* **1991**, *124* (2), 333−336. (b) Gómez-Benítez, V.; Baldovino-Pantaleón, O.; Herrera-Álvarez, C.; Toscano, R. A.; Morales-Morales, D. High yield thiolation of iodobenzene catalyzed by the phosphinite nickel PCP pincer complex: [NiCl{C6H3−2,6-(OPPh2)2}]. *Tetrahedron Lett.* **2006**, *47* (29), 5059−5062. (c) Gutsulyak, D. V.; Piers, W. E.; Borau-Garcia, J.; Parvez, M. Activation of Water, Ammonia, and Other Small Molecules by PCcarbeneP Nickel Pincer Complexes. *J. Am. Chem. Soc.* **2013**, *135* (32), 11776−11779. (d) Jonasson, K. J.; Wendt, O. F. Synthesis and Characterization of a Family of POCOP Pincer Complexes with Nickel: Reactivity Towards CO2 and Phenylacetylene. *Chem. - Eur. J.* **2014**, *20* (37), 11894−11902. (e) Jonasson, K. J.; Wendt, O. F. Synthesis and characterisation of new PCsp3P-supported nickel complexes. *J. Organomet. Chem.* **2014**, *759*, 15−18. (f) Mousa, A. H.; Bendix, J.; Wendt, O. F. Synthesis, Characterization, and Reactivity of PCN Pincer Nickel Complexes. *Organometallics* **2018**, *37* (15), 2581−2593. (g) Zargarian, D.; Castonguay, A.; Spasyuk, D. M., ECE-Type Pincer Complexes of Nickel. In *Organometallic Pincer Chemistry*; van Koten, G., Milstein, D., Eds.; Springer Berlin Heidelberg: Berlin, Heidelberg, 2013; pp 131−173. (h) Castonguay, A.; Beauchamp, A. L.; Zargarian, D. New Derivatives of PCP-Type Pincer Complexes of Nickel. *Inorg. Chem.* **2009**, *48* (7), 3177−3184. (i) Vabre, B.; Canac, Y.; Duhayon, C.; Chauvin, R.; Zargarian, D. Nickel(II) complexes of the new pincer-type unsymmetrical ligands PIMCOP, PIMIOCOP, and NHCCOP: versatile binding motifs. *Chem. Commun.* **2012**, *48* (84), 10446−10448. (j) Hao, J.; Mougang-Soumé, B.; Vabre, B.; Zargarian, D. On the Stability of a POCsp3OP-Type Pincer Ligand in Nickel(II) Complexes. *Angew. Chem.* **2014**, *126* (12), 3282−3286. (k) Vabre, B.; Petiot, P.; Declercq, R.; Zargarian, D. Fluoro and Trifluoromethyl Derivatives of POCOP-Type Pincer Complexes of Nickel: Preparation and Reactivities in SN_2 Fluorination and Direct Benzylation of Unactivated Arenes. *Organometallics* **2014**, *33* (19), 5173−5184.

(7) (a) Lefèvre, X.; Durieux, G.; Lesturgez, S.; Zargarian, D. Addition of amines and phenols to acrylonitrile derivatives catalyzed by the POCOP-type pincer complex [{κP,κC,κP-2,6-(i-Pr2PO)-2C6H3}Ni(NCMe)][OSO2CF3]. *J. Mol. Catal. A: Chem.* **2011**, *335* (1), 1−7. (b) Hao, J.; Vabre, B.; Mougang-Soumé, B.; Zargarian, D. Small Molecule Activation by POCOP-Nickel Complexes. *Chem. - Eur. J.* **2014**, *20* (39), 12544−12552. (c) Salah, A.; Corpet, M.; ul-Hassan Khan, N.; Zargarian, D.; Spasyuk, D. M. Synthesis of unsymmetrical 5,6-POCOP′-type pincer complexes of nickel(ii): impact of nickelacycle size on structures and spectroscopic properties. *New J. Chem.* **2015**, *39* (8), 6649−6658.

(8) Vabre, B.; Deschamps, F.; Zargarian, D. Ortho Derivatization of Phenols through C−H Nickelation: Synthesis, Characterization, and Reactivities of Ortho-Nickelated Phosphinite Complexes. *Organometallics* **2014**, *33* (22), 6623−6632.

(9) Mangin, L. P.; Zargarian, D. C−H nickelation of phenol-derived phosphinites: regioselectivity and structures of cyclonickelated complexes. *Dalton Transactions* **2017**, *46* (46), 16159−16170.

(10) Vabre, B.; Lambert, M. L.; Petit, A.; Ess, D. H.; Zargarian, D. Nickelation of PCP- and POCOP-Type Pincer Ligands: Kinetics and Mechanism. *Organometallics* **2012**, *31* (17), 6041−6053.

(11) (a) Baho, N.; Zargarian, D. Diphenyl(dipyrazolyl)methane Complexes of Ni: Synthesis, Structural Characterization, and Chromotropism of NiBr2 Derivatives. *Inorg. Chem.* **2007**, *46* (18), 7621−7632. (b) Lapointe, S.; Vabre, B.; Zargarian, D. POCOP-Type Pincer Complexes of Nickel: Synthesis, Characterization, and Ligand Exchange Reactivities of New Cationic Acetonitrile Adducts. *Organometallics* **2015**, *34* (14), 3520−3531. (c) Lefèvre, X.; Spasyuk, D. M.; Zargarian, D. *J. Organomet. Chem.* **2011**, *696*, 864−870. (d) Wang, R.; Groux, L. F.; Zargarian, D. Nickel-Triflate Complexes as Precursors to Reactive Cations: Preparation and Reactivities of (1-R-indenyl)Ni(PPh3)(OSO2CF3). *Organometallics* **2002**, *21* (25), 5531−5539. (e) Spasyuk, D. M.; Gorelsky, S. I.; van der Est, A.; Zargarian, D. Characterization of Divalent and Trivalent Species Generated in the Chemical and Electrochemical Oxidation of a Dimeric Pincer Complex of Nickel. *Inorg. Chem.* **2011**, *50*, 2661−2674. (f) Groux, L. F.; Zargarian, D. Aminoalkyl-Substituted Indenyl−Nickel Compounds: Tuning Reactivities as a Function of the Pendant, Hemilabile Moiety. *Organometallics* **2003**, *22* (15), 3124−3133.

(12) This complex has been shown to adopt a square -planar structure in the solid state. See ref 9 for its preparation, isolation, and solid-state characterization.

(13) It should be noted that EtOAc and THF mixtures showed the same colors as the toluene mixtures; to simplify the discussion, we have focused on toluene mixtures.

(14) The rates of these reactions were monitored by observing the emergence of ^{31}P signals characteristic of the cyclonickelated complexes: a singlet at 196 ppm in acetonitrile for (κ^P,κ^C-*i*-$Pr_2POC_6H_4$)Ni(NCMe)Br and AB doublets at 184 and 151 ppm in toluene for (κ^P,κ^C-*i*-$Pr_2POC_6H_4$)Ni(*i*-Pr_2POPh)Br. Complete conversion was noted by the complete disappearance of the broad signals due to the nonmetalated phosphinite adducts, whereas partial conversions were estimated by integration of the signals for the metalated and nonmetalated species.

(15) Since toluene samples of both the starting material *trans*-L_2NiBr_2 and the cyclometalated product (κ^P,κ^C-*i*-$Pr_2POC_6H_4$)Ni(*i*-Pr_2POPh)Br display sharp ^{31}P signals, the extent of cyclometalation in toluene mixtures could be determined in a straightforward manner on

DOI: 10.1021/acs.organomet.8b00899
Organometallics XXXX, XXX, XXX−XXX

the basis of NMR. In the case of the reactions conducted in acetonitrile, however, determination of conversion is complicated by the fact that the ^{31}P NMR spectrum of the reaction mixture displays no signals due to the ligand substitution reaction between the cyclometalated complex and the solvent. In this case, conversions were determined by evaporating the final mixture, dissolving the solid residues in toluene, and recording the ^{31}P NMR of this sample.

(16) It should be noted that the experimental m/z values obtained from this analysis correspond to "$M^+ - 1$" for the parent ion with one Ni-bound MeCN, $M^+ = [C_{17}H_{30}Br_2N_2NiOP]^+ = 526.98$, and to "$M^+ + 2$" for the parent ion with two Ni-bound MeCN, $M^+ = [C_{19}H_{33}Br_2N_3NiOP]^+ = 568.01$. Of course, we are mindful of the fact that the highly dilute solutions required for ESI-MS experiments would be expected to affect the equilibria governing the speciation of Ni, which might cast doubt on the relevance of this result for the overall reaction mechanism under realistic reaction conditions. This result is nevertheless significant, because it supports the viability of a monophosphinite adduct in MeCN.

(17) (a) Paulsen, H.; Duelund, L.; Winkler, H.; Toftlund, H.; Trautwein, A. X. Free Energy of Spin-Crossover Complexes Calculated with Density Functional Methods. *Inorg. Chem.* **2001**, *40* (9), 2201−2203. (b) Reiher, M.; Salomon, O.; Artur Hess, B. Reparameterization of hybrid functionals based on energy differences of states of different multiplicity. *Theor. Chem. Acc.* **2001**, *107* (1), 48−55. (c) Reiher, M. Theoretical Study of the $Fe(phen)_2(NCS)_2$ Spin-Crossover Complex with Reparametrized Density Functionals. *Inorg. Chem.* **2002**, *41* (25), 6928−6935. (d) Conradie, J.; Ghosh, A. DFT Calculations on the Spin-Crossover Complex Fe(salen)(NO): A Quest for the Best Functional. *J. Phys. Chem. B* **2007**, *111* (44), 12621−12624.

(18) See calculations on page S23 of the Supporting Information, which were based on these references: (a) Raamat, E.; Kaupmees, K.; Ovsjannikov, G.; Trummal, A.; Kütt, A.; Saame, J.; Koppel, I.; Kaljurand, I.; Lipping, L.; Rodima, T.; Pihl, V.; Koppel, I. A.; Leito, I. Acidities of strong neutral Brønsted acids in different media. *J. Phys. Org. Chem.* **2013**, *26* (2), 162−170. (b) Kaljurand, I.; Kütt, A.; Sooväli, L.; Rodima, T.; Mäemets, V.; Leito, I.; Koppel, I. A. Extension of the Self-Consistent Spectrophotometric Basicity Scale in Acetonitrile to a Full Span of 28 pKa Units: Unification of Different Basicity Scales. *J. Org. Chem.* **2005**, *70* (3), 1019−1028.

(19) (a) Vabre, B.; Spasyuk, D. M.; Zargarian, D. Impact of Backbone Substituents on POCOP-Ni Pincer complexes: A Structural, Spectroscopic and Electrochemical Study. *Organometallics* **2012**, *31* (24), 8561−8570. (b) Vabre, B.; Lindeperg, F.; Zargarian, D. Direct, one-pot synthesis of POCOP-type pincer complexes from metallic nickel. *Green Chem.* **2013**, *15* (11), 3188−3194.

(20) Zhao, Y.; Truhlar, D. G. The M06 suite of density functionals for main group thermochemistry, thermochemical kinetics, noncovalent interactions, excited states, and transition elements: two new functionals and systematic testing of four M06-class functionals and 12 other functionals. *Theor. Chem. Acc.* **2008**, *120* (1), 215−241.

(21) Raju, R. K.; Bengali, A. A.; Brothers, E. N. A unified set of experimental organometallic data used to evaluate modern theoretical methods. *Dalton Transactions* **2016**, *45* (35), 13766−13778.

(22) (a) Lee, C.; Yang, W.; Parr, R. G. Development of the Colle-Salvetti correlation-energy formula into a functional of the electron density. *Phys. Rev. B: Condens. Matter Mater. Phys.* **1988**, *37* (2), 785−789. (b) Becke, A. D. Density-functional thermochemistry. III. The role of exact exchange. *J. Chem. Phys.* **1993**, *98* (7), 5648−5652.

(23) Legault, C. Y. *CYLview, 1.0b*; Université de Sherbrooke, 2009; http://www.cylview.org.

DOI: 10.1021/acs.organomet.8b00899
Organometallics XXXX, XXX, XXX−XXX